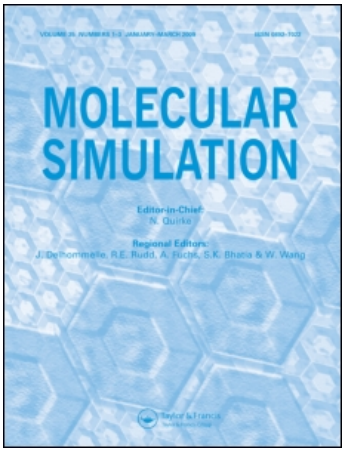

Molecular Simulation
Publication details, including instructions for authors and subscription information:
http://www.informaworld.com/smpp/title~content=t713644482

The Implementation of the Iterative Diagonalization Scheme and *ab initio* Molecular Dynamics Simulation with the LAPW Method

Kentaro Uehara[a]; John S. Tse[a]
[a] Steacie Institute for Molecular Science, National Research Council of Canada, Ottawa, Ontario, Canada

To cite this Article Uehara, Kentaro and Tse, John S.(2000) 'The Implementation of the Iterative Diagonalization Scheme and *ab initio* Molecular Dynamics Simulation with the LAPW Method', Molecular Simulation, 23: 6, 343 — 361
To link to this Article: DOI: 10.1080/08927020008023008
URL: http://dx.doi.org/10.1080/08927020008023008

Molecular Simulation, 2000, Vol. 23, pp. 343–361
Reprints available directly from the publisher
Photocopying permitted by license only

THE IMPLEMENTATION OF THE ITERATIVE DIAGONALIZATION SCHEME AND *AB INITIO* MOLECULAR DYNAMICS SIMULATION WITH THE LAPW METHOD

KENTARO UEHARA and JOHN S. TSE*

Steacie Institute for Molecular Science, National Research Council of Canada, Ottawa, Ontario, Canada K1A 0R6

(Received September 1999; accepted October 1999)

A new *ab initio* molecular dynamics method based on the full-potential linearized-augmented-plane-wave (LAPW) basis set has been implemented. The LAPW basis set has been successfully employed for systems containing localized electrons such as first row atoms and transition metals. In our implementation of the LAPW-MD scheme, iterative residual minimization algorithm is used to solve the electronic states problem. The atoms are moved according to forces derived from the Hellman–Feynman theorem and incomplete basis set correction terms. The performance of the program is further enhanced by parallelization. We will discuss technical details of the program implementation and present results obtained from this code to the equilibrium structures and vibrational properties of simple diatomic molecules.

Keywords: LAPW-MD; Hellman–Feynman theorem; *ab initio* molecular dynamics

PACs numbers: 02.70.-c, 07.05.Tp, 31.15.Ar, 31.15.Og

1. INTRODUCTION

The linearized-augmented-plane-wave (LAPW) method [1,2] is one of the most accurate all-electron method. Within the framework of density functional theory [3–6], this method has been applied to a wide range of solid state systems and yielded very accurate electronic structure, total energy, bulk modulus and so on [7–10]. Recently, Yu *et al.* [11] derived a

*Corresponding author.

practical representation of the atomic forces for the LAPW method. These expressions have been implemented in some LAPW codes and the equilibrium geometries and vibrational frequencies obtained using these force formulae show good agreement with the experiments and the theoretical results.

One of the prominent features of the LAPW method is its ability of optimizing basis sets in accordance with the change of the local potential profile. In contrast, the standard pseudopotential method suffers from the problem of transferability in the case when a large change of local environment from reference system takes place. Such a large change is expected to be present in some cases, *e.g.*, chemical reactions, photoactivation processes, where the chemical state of the element may be altered. An *ab initio* molecular dynamics (AIMD) simulation is an excellent tool to investigate the systems in which dynamics of the ions and the electronic properties are strongly correlated. Therefore, it is expected that the combination of the LAPW method and molecular dynamics (MD) simulation would provide a very useful tool in these particularly difficult cases.

One of the most challenging systems for the LAPW method is the first row transition metal clusters. To our knowledge, there are few application on the cluster systems studied by the LAPW method. The difficulties associated with the cluster systems mainly come from the need of small muffin tin (MT) radii R_{MT} and the use of large supercell box. In a LAPW calculation, the product of the MT radius and the magnitude of maximum wave vector $R_{MT}K_{max}$ roughly determines the quality of the calculation. The value usually lies between 7.5 to 10. Therefore a small MT radius increase the number of plane-wave (PW) coefficients [2]. Furthermore, a large super-cell simulation box requires many PW's because of the periodic boundary condition imposed on the wave functions.

It is well known that the cost of matrix diagonalization process is proportional to N_{pw}^3, where the N_{pw} represents a number of plane waves. In the conventional LAPW method, explicit matrix diagonalization is often used to solve the eigenvalue problem. Thus, a large scale calculation using the conventional LAPW method will become prohibitively expensive. In order to overcome this difficulty, we have adopted the iterative diagonalization scheme to the LAPW method.

The iterative diagonalization scheme is the preferred technique for large scale electronic structure calculations and an AIMD simulations. As we will show in Section 3, it is possible to carry out Car-Parrinello (CP) type AIMD [12] using the LAPW method. However, in this case, the number of operations involving the manipulation of the overlap matrix scales as $O(N_{pw}^3)$. Among several iterative diagonalization schemes, conjugate gradient

(CG) [13, 14] and 'residual minimization/direct inversion in the iterative subspace' (RMM-DIIS) methods [15–18] exhibit very good convergence properties. The CG method optimizes wave functions by searching in conjugate direction, whereas the RMM-DIIS scheme directly minimizes the residual vector.

This paper is organized as follows. In Section 2, we will briefly describe representation of the LAPW wave function, Hamiltonian and overlap matrix elements using projector method. In Section 3, implementation of the iterative diagonalization schemes to the LAPW method will be discussed. Numerical results on simple diatomic molecules will be presented in Section 6. We will discuss parallel efficiency using a different approach in Section 7.

2. LAPW METHOD

2.1. Wave Function

A non-orthogonal basis set is used in the LAPW method. A LAPW wave function is simply written as,

$$\psi(\mathbf{r}) = \sum_G c_G \phi_G(\mathbf{r}). \tag{1}$$

The LAPW basis set $\phi_G(\mathbf{r})$ is equivalent to planewave in the interstitial (IST) region and similar to the atomic eigenfunction in the muffin-tin (MT) region.

$$\phi_G(\mathbf{r}) = \exp(i\mathbf{G}\cdot\mathbf{r})\Theta(\mathbf{r}\in \text{IST}) + \sum_n \Theta_n(\mathbf{r}\in n'\text{th MT}) \sum_{lm} [a^n_{lm}(\mathbf{G})u^n_l(r) + b^n_{lm}(\mathbf{G})\dot{u}^n_l(r)]Y_{lm}(\hat{\mathbf{r}}) \tag{2}$$

where $\Theta(\mathbf{r})$ represents a step function, which is unity in the defined region and zero otherwise, $u^n_l(r)$ and $\dot{u}^n_l(r)$ are the solutions of the radial Schrödinger equation and its energy derivative respectively. Linear coefficients $a^n_{lm}(\mathbf{G})$ and $b^n_{lm}(\mathbf{G})$ appearing in Eq. (2) are determined by the boundary conditions imposed on the wave functions

$$\psi_{\text{IST}}(\vec{r})|_{|r|=R^n_{\text{MT}}} = \psi_{\text{MT}}(\vec{r})|_{|r|=R^n_{\text{MT}}} \tag{3}$$

$$\frac{\partial}{\partial \mathbf{r}}\psi_{\text{IST}}(\mathbf{r})\bigg|_{|r|=R^n_{\text{MT}}} = \frac{\partial}{\partial \mathbf{r}}\psi_{\text{MT}}(\mathbf{r})\bigg|_{|r|=R^n_{\text{MT}}} \tag{4}$$

These conditions guarantee that the wave functions are smoothly connected on the n'th MT sphere surface up to first derivative. Substituting Eqs. (1), (2) into Eqs. (3) and (4), we obtain the expressions for the linear coefficients $a^n_{lm}(\mathbf{G})$ and $b^n_{lm}(\mathbf{G})$,

$$a^n_{lm}(\mathbf{G}) = e^{i\mathbf{G}\cdot\mathbf{R}_n}\left[p^1_{lm,n}(\mathbf{G})\frac{\partial \dot{u}^n_l}{\partial r}\bigg|_{r=R^n_{\mathrm{MT}}} - p^2_{lm,n}(\mathbf{G})\dot{u}^n_l(R^n_{\mathrm{MT}})\right]\Big/\Delta \tag{5}$$

$$b^n_{lm}(\mathbf{G}) = e^{i\mathbf{G}\cdot\mathbf{R}_n}\left[-p^1_{lm,n}(\mathbf{G})\frac{\partial u^n_l}{\partial r}\bigg|_{r=R^n_{\mathrm{MT}}} + p^2_{lm,n}(\mathbf{G})u^n_l(R^n_{\mathrm{MT}})\right]\Big/\Delta \tag{6}$$

$$\Delta = u^n_l(R^n_{\mathrm{MT}})\frac{\partial \dot{u}^n_l}{\partial r}\bigg|_{r=R^n_{\mathrm{MT}}} - \dot{u}^n_l(R^n_{\mathrm{MT}})\frac{\partial u^n_l}{\partial r}\bigg|_{r=R^n_{\mathrm{MT}}} \tag{7}$$

where $p^1_{lm,n}$ and $p^2_{lm,n}$ are the analytical projector functions [19, 20] that consist of spherical Bessel functions $j_l(GR_n)$ and spherical harmonics $Y_{lm}(\hat{\mathbf{G}})$,

$$p^1_{lm,n}(\mathbf{G}) = 4\pi i^l j_l(GR^n_{\mathrm{MT}})Y^*_{lm}(\hat{\mathbf{G}}) \tag{8}$$

$$p^2_{lm,n}(\mathbf{G}) = \frac{4\pi i^l G}{2l+1}[lj_{l-1}(GR^n_{\mathrm{MT}}) - (l+1)j_{l+1}(GR^n_{\mathrm{MT}})]Y^*_{lm}(\hat{\mathbf{G}}) \tag{9}$$

The Hamiltonian $\mathrm{H}_{G,G'} \equiv \langle G|\mathrm{H}|G'\rangle$ and overlap matrices $S_{G,G'} \equiv \langle G|G'\rangle$ are represented as

$$\begin{aligned}\mathrm{H}_{G,G'} = {} & \Omega\frac{1}{2}\delta_{G,G'}G^2 - \frac{1}{2}\mathbf{G}F(\mathbf{G}-\mathbf{G}')\mathbf{G}' \\ & + \int V(\mathbf{r})\Theta(\mathbf{r}\in \mathrm{IST})e^{-i(\mathbf{G}-\mathbf{G}')\cdot\mathbf{r}}d\mathbf{r} \\ & + \sum_n\sum_{lm}\sum_{l'm'}\sum_{\kappa,\kappa'} e^{-i(\mathbf{G}-\mathbf{G}')\cdot\mathbf{R}_n}p^{\kappa *}_{lm,n}(\mathbf{G})\mathrm{H}^{\kappa,\kappa'}_{lm,l'm',n}p^{\kappa'}_{l'm',n}(\mathbf{G}')\end{aligned} \tag{10}$$

$$\begin{aligned}S_{G,G'} = {} & \Omega\delta_{G,G'} - F(\mathbf{G}-\mathbf{G}') \\ & + \sum_n\sum_{lm}\sum_{\kappa,\kappa'} e^{-i(\mathbf{G}-\mathbf{G}')\cdot\mathbf{R}_n}p^{\kappa *}_{lm,n}(\mathbf{G})S^{\kappa,\kappa'}_{lm,n}p^{\kappa'}_{lm,n}(\mathbf{G}')\end{aligned} \tag{11}$$

where

$$F(\mathbf{G}) \equiv \sum_n e^{-i\mathbf{G}\cdot\mathbf{R}_n}\int_n e^{-i\mathbf{G}\cdot\mathbf{r}}d\mathbf{r} \tag{12}$$

$$S^{\kappa,\kappa'}_{lm,n} \equiv \int_0^{R^n_{\mathrm{MT}}} u^{n,\kappa}_l(r)u^{n,\kappa'}_l(r)r^2dr \tag{13}$$

$$H^{\kappa,\kappa'}_{lm,l'm',n} \equiv \delta_{l,l'}\delta_{m,m'}\frac{1}{2}\left\{\int_0^{R^n_{\mathrm{MT}}} \frac{\partial u_l^{n,\kappa}(r)}{\partial r}\frac{\partial u_l^{n,\kappa'}(r)}{\partial r} r^2 dr + l(l+1)\int_0^{R^n_{\mathrm{MT}}} u_l^{n,\kappa}(r)u_l^{n,\kappa'}(r)dr\right\} + \int_0^{R^n_{\mathrm{MT}}} u_l^{n,\kappa}(r)Y^*_{lm}(\hat{\mathbf{r}})V(\mathbf{r})Y_{l'm'}(\hat{\mathbf{r}})u_{l'}^{n,\kappa'}(r)d\mathbf{r} \tag{14}$$

The all-electron potential $V(\mathbf{r})$ in Eq. (10) includes the electrostatic potential and exchange-correlation potential [8, 2].

For heavy elements with atomic number $Z \geq 50$, relativistic effects become important. In the conventional LAPW method, the wave function is treated relativistically in the MT region and non-relativistically in the interstitial region. This treatment is reasonable because the electrons near the MT surface have small velocity in comparison with the ones near the nucleus. The Dirac's equation is used to solve the radial wave function in the relativistic case [21]. On the MT surface, only the major component of the solution of the Dirac's equation is considered to be connected with the interstitial wave functions. The minor component normally has a very small magnitude on the MT surface.

3. ITERATIVE DIAGONALIZATION SCHEME

When a large number of basis functions are involved in a electronic structure calculation, the explicit matrix diagonalization process consumes a lot of CPU time. In addition, the memory space required to store the Hamiltonian and the overlap matrices quickly grows to more than a few giga-bytes. The conventional LAPW method explicitly constructs the Hamiltonian and overlap matrices. The number of operation for both of these process are proportional to N_{pw}^2. Furthermore, the CPU time of the diagonalization process grows as $O(N_{pw}^3)$. On the other hand, Car-Parrinello (CP) type calculation requires neither the explicit diagonalization of Hamiltonian nor the huge matrices arrays in a program code. The scaling property of standard CP calculation is $O(N_{pw}\log N_{pw})$ for the iterative diagonalization process and $O(N_{pw})$ for memory usage. Goedecker *et al.* [20] have recently shown a method for an efficient matrix-vector multiplication in the LAPW method. The time consuming part in the Hamiltonian matrix-vector product is calculated by a convolution technique using fast Fourier transformation (FFT). When we adopt this scheme, the total operation count is lowered to $O(N_{pw}\log N_{pw})$ and no storage of large matrix arrays is necessary.

3.1. Car-Parrinello Type Scheme

When the basis set is non-orthogonal, the overlap matrix appears on both sides of the Car-Parrinello's equation [12]

$$\mu \mathbf{S}|\ddot{\psi}\rangle = -(\mathbf{H} - \varepsilon \mathbf{S})|\psi\rangle. \tag{15}$$

where $\mathbf{H}_{G,G'} \equiv \langle G|\mathrm{H}|G'\rangle$, $\mathbf{S} \equiv \langle G|G'\rangle$ and $\varepsilon = \langle\psi|\mathrm{H}\psi\rangle/\langle\psi|\psi\rangle$. In order to transform Eq. (15) to a symmetric form with respect to $|\psi\rangle$, we decompose the overlap matrix into the form $\mathbf{S} = \mathbf{U}^{\dagger}\mathbf{U}$. This process is called Choleski decomposition [22] and most numerical library packages contain this routine. Substituting the decomposed form into Eq. (15) and multiplying by $\mathbf{U}^{\dagger^{-1}}$ from the left hand side, we obtain

$$\mu \mathbf{U}|\ddot{\psi}\rangle = -(\mathbf{U}^{\dagger^{-1}}\mathbf{H}\mathbf{U}^{-1} - \varepsilon)\mathbf{U}|\psi\rangle \tag{16}$$

Equation (16) can be rewritten as

$$\mu|\ddot{\psi}\rangle' = -(\mathbf{H}' - \varepsilon)|\psi\rangle' \tag{17}$$

where

$$|\psi\rangle' \equiv \mathbf{U}|\psi\rangle, \quad \mathbf{H}' \equiv \mathbf{U}^{\dagger^{-1}}\mathbf{H}\mathbf{U}^{-1} \tag{18}$$

Equation (17) has the same form as in the case of an orthogonal basis set. Therefore, based on the Eqs. (17) and (18) we can use same methodology of the CP method.

We have implemented the damped Newtonian dynamics [23] method to optimize the wave function in the LAPW code. The damped Newtonian dynamics equation is written as

$$\mu\ddot{\psi}(\mathbf{r}) = -(\mathrm{H} - \varepsilon)\psi(\mathbf{r}) - 2\eta\mu\dot{\psi}(\mathbf{r}) \tag{19}$$

where μ and η are fictitious mass and damping coefficient, respectively. A large value of η value results in slow convergence near the quadratic energy region, whereas a smaller η value approaches to the steepest descent (SD) method. Therefore, we must choose an appropriate value of η at every quenching step, *i.e.*, a small η at early steps and a large η in the quadratic region. The value of η at the i'th quenching step is determined using the total energy at three preceding successive steps,

$$\eta_{i+1} = \begin{cases} \frac{1}{\Delta t}\sqrt{\frac{1}{2}\ln\left(\frac{\Delta E_{i-1}}{\Delta E_i}\right)} & \Delta E_{i-1}/\Delta E_i > 1 \\ \eta_i + \Delta\eta & \text{Otherwise} \end{cases} \tag{20}$$

where $\Delta E_i \equiv E_{i-1} - E_i$ and $\Delta\eta$ represents the increase in the value of η. We chose the $\Delta\eta$ to be 5% of the η value at a particular early step. The value of η is increased while the second condition of Eq. (20) is applied. When the first condition is applied, *i.e.*, in the case of overdamping, η_{i+1} is compared with η_i and adopted as a new damping coefficient if η_{i+1} is smaller than η_i. $\Delta\eta$ is also re-evaluated when the condition of overdamping is applied.

Figure 1 shows the comparison of total energy convergence between the SD method and the damped Newtonian dynamics method. In this calculation, a 8 atom diamond structure Si fcc unit cell is used and the initial wave functions and charge density are generated from random number sequences. At the early steps, the convergence rate of the both method is same. It is because in the first 10 iteration η was set to be zero in order to find the optimal value of η by running with the SD method. After the 10th iteration, the optimal value of η was set and η was updated every 5 iteration steps so as to achieve a good energy convergence rate. As it can be clearly seen from Figure 1, the damped Newtonian dynamics method has a great advantage compared with the SD method. Note that the operation cost of the Choleski decomposition is $O(N_{pw}^3)$. This implies, as long as we use the Choleski decomposition, there is no advantage compared with the explicit diagonalization scheme.

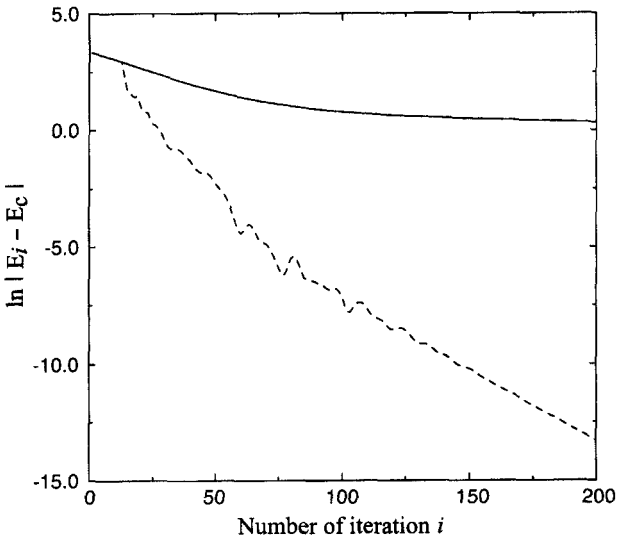

FIGURE 1 The evolution of total energy measured from converged total energy E_c for diamond structure Si crystal. Solid line corresponds to steepest descent method and dashed line corresponds to damped Newtonian dynamics method.

3.2. RMM-DIIS Method

Here we define the residue as

$$R(\mathbf{r}) = (\mathrm{H} - \varepsilon)\psi(\mathbf{r}). \tag{21}$$

If we expand the residue and wave function using the non-orthogonal basis set $\{\psi(\mathbf{G})\}$, we obtain the matrix and vector notation of Eq. (21)

$$\mathbf{S}|R\rangle = (\mathbf{H} - \varepsilon\mathbf{S})|\psi\rangle \tag{22}$$

Therefore the task of solving the eigenvalue problem is transformed to the search for a point in the phase space where the magnitude of residual vector becomes zero.

The RMM-DIIS method minimizes the residual vector iteratively. At the $(m+1)$th step of iteration, a new trial vector is calculated from the linear combination of preceding trial vectors and the initial guess of the eigenfunction,

$$\left|\psi^{(m+1)}\right\rangle = \sum_{j=0}^{m} \alpha_j \left|\xi^{(j)}\right\rangle \tag{23}$$

where we assume $|\xi^{(j=0)}\rangle$ is identical to the initial wave function $|\psi^{(0)}\rangle$. The linear coefficients $\{\alpha_j\}$ are obtained by solving an eigenvalue problem

$$\mathbf{A}|\alpha\rangle = \eta^2\mathbf{B}|\alpha\rangle \tag{24}$$

The matrix elements of **A** and **B** are defined as

$$A_{ij} = \langle(\mathbf{H} - \varepsilon\mathbf{S})\xi^{(i)}|(\mathbf{H} - \varepsilon\mathbf{S})\xi^{(j)}\rangle \tag{25}$$

$$B_{ij} = \langle\xi^{(i)}|\mathbf{S}|\xi^{(j)}\rangle. \tag{26}$$

where the ε is an eigenvalue of the trial wave function and the lowest eigenvalue of Eq. (24) corresponds to the square of the norm of the residual vector. Substituting the lowest eigenvector into Eq. (23) yields the new trial vector which minimizes the residue. Note that this procedure only gives the point in which the norm of residual vector is minimum, *i.e.*, the RMM-DIIS method does not guarantee the norm of residual vector converges to zero. In order to circumvent the problem of sticking in a quasi-minimum, we must choose the initial wave vector to be close to the quadratic region of the energy surface.

The dimension of the matrices in Eqs. (25) and (26) is $(N_{it}+1)^2$, where N_{it} is a number of iterations that has a value of at most $10 \sim 15$, so the computational cost of the diagonalization is negligible in comparison with the other part of the SCF cycle.

The flowchart of the band structure calculation using RMM-DIIS scheme is depicted in Figure 3. At the initialization step, charge density is initialized by the overlapping of free atom's charge densities. After the calculation of the charge density, the electrostatic potential $V_H(r)$ and exchange-correlation potential $V_{XC}(r)$ are evaluated on the real space grid. In the next step, the RMM-DIIS scheme is used to quench the wave functions onto the Born-Oppenheimer (BO) surface. Usually, the number of the RMM-DIIS iteration steps required is within 5 to 7. After the residuals of all the band satisfy the convergence criterion, the core states and the basis set is updated by solving the radial Schrödinger equation. Finally, the input charge density for the next iterative step is calculated by mixing the new charge density and old charge density using the Broyden's II method [24]. This self-consistent loop is repeated until the convergence criterion for the total energy is satisfied.

One of the significant features of the RMM-DIIS method is that there is no need to orthogonalize the wave functions explicitly during the iterative diagonalization. As it has been pointed out by several authors, the computational cost of an explicit orthogonalization, such as a Gram-

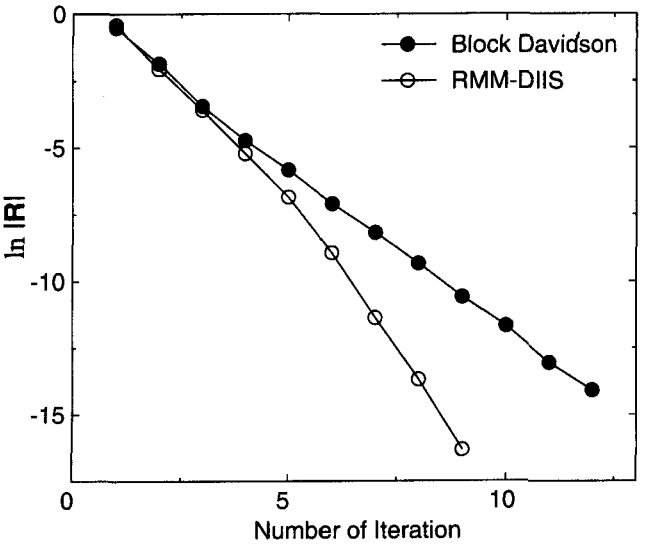

FIGURE 2 Comparison of convergence efficiency between block Davidson (solid line with filled circle) and RMM-DIIS scheme (solid line with open circle).

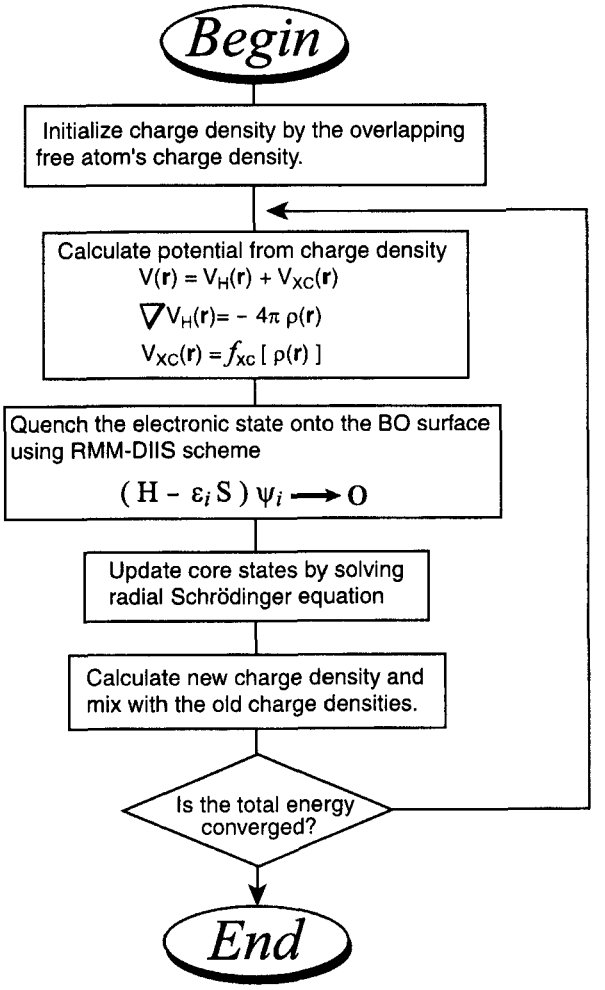

FIGURE 3 Flowchart of self-consistent cycle of LAPW calculation using the RMM-DIIS scheme.

Schmidt diagonalization scheme, scales as $O(N^3)$ (N: system size), and it might become a serious problem when carried out on large system calculation. Thus, it is preferable to avoid the orthogonalization process if possible. Another good aspect of the RMM-DIIS method is that the each band is optimized independently since there is no need to orthogonalize the current band to the other bands. This feature allows us to make band parallel code easily. We will discuss the parallel efficiency of the RMM-DIIS later.

Figure 2 shows evolution of the residual vector of block Davidson and RMM-DIIS scheme for diamond Si system. In this case, the initial wave function was taken from the result of a few iteration using SD method. At the 9th iteration step, the absolute value of the residual vector obtained from the RMM-DIIS scheme is smaller than the block Davidson scheme by around an order of 6.

4. SPIN POLARIZATION CALCULATION

For open shell systems, we employed spin unrestricted calculations where the α- and β-spin states are treated separately. The local spin exchange-correlation potential (V_{xc}) is calculated for each spin component and contributes to the potential energy terms of the Hamiltonian. In the electronic states quenching process, the wavefunctions are quenched separately for each spin component. The Fermi energy is calculated at the end of every SCF steps to evaluate the fractional occupancy of the bands. We have implemented both the finite temperature Fermi distribution function and Gaussian smearing for the calculation of the fractional occupancies.

$$f_{\text{Fermi}}(\varepsilon) = \frac{1}{1 + \exp((\varepsilon - \varepsilon_F)/\sigma)} \tag{27}$$

$$f_{\text{Gaussian}}(\varepsilon) = \frac{1}{2}\text{Erfc}\left(\frac{\varepsilon - \varepsilon_F}{\sigma}\right). \tag{28}$$

Here ε_F, σ and Erfc represent Fermi energy, smearing width of the Fermi distribution and complementary error function respectively. Several unoccupied states are included to take into account the fractional occupancy.

The total number of electrons is calculated by summing over band occupancies f_i from the lowest level.

$$\tilde{N}_{el} = \sum_{i}^{N_{\text{band}}} f_i \tag{29}$$

Initially, the Fermi energy is assumed to be the midpoint between the lowest occupied and highest unoccupied eigenvalue. Then we calculate $\tilde{N}_{el}$ and move the Fermi energy according to the sign of $\tilde{N}_{el} - N_{el}$, where N_{el} represents the true number of total electrons. This procedure is repeated until $|\tilde{N}_{el} - N_{el}|$ satisfies the convergence criterion.

5. IMPLEMENTATION OF THE MOLECULAR DYNAMIC SCHEME

Here we describe the implementation of AIMD simulation using the LAPW basis set. The Car-Parrinello method, the pioneering technique for AIMD simulation, has been applied to many systems, including bulk solids, surfaces and molecules. As we mentioned earlier, in principle it is possible to implement the CP method by means of the non-orthogonal basis set. However, in a large system, the existence of the overlap matrix results in $O(N_{pw}^3)$ scaling in the wave function updating process.

Apart from CP method, the AIMD using CG or RMM-DIIS iterative diagonalization scheme has been recognized as a good alternative to the CP method. It has two significant features. First, the MD time step can be taken much larger (by even more than a factor of 10) than that of the CP method. Secondly, it does not have any difficulty in the case of small band gap systems or metallic systems, whereas in the CP method, the MD time step is restricted by the nature of the electronic structure because the ionic and the electronic degrees of freedom are treated in the same way. For these reasons, we chose the RMM-DIIS iterative diagonalization based AIMD and implemented it using the LAPW basis set.

A flowchart of the molecular dynamics calculation is depicted in Figure 4. At the initialization step, wave functions and charge densities are fully optimized by the iterative diagonalization. Next, we proceed to the MD loop. The atoms are moved according to the Hellman–Feynman and incomplete basis set correction forces [11]. The incomplete basis set correction consists of core and valence contributions. The velocity Verlet method is employed to integrate the equation of motion for the atoms. Then the charge density is extrapolated to obtain a good initial guess of the charge density for the next MD step. The second order extrapolation formula is used when the MD step is greater than 2, and a lower order relation is used in the other cases.

$$\rho_{i+1}(\mathbf{r}) = \rho_i(\mathbf{r}) + 2[\rho_i(\mathbf{r}) - \rho_{i-1}(\mathbf{r})] - [\rho_{i-1}(\mathbf{r}) - \rho_{i-2}(\mathbf{r})] \tag{30}$$

Note that the LAPW wave functions are not extrapolated because the basis set has changed during the consecutive MD steps, so we used the converged wave functions of the previous MD step as an initial guess of the wave functions in the subsequent step.

The extrapolated charge density and the initial guess of the wave functions are quenched onto new BO surface using the RMM-DIIS scheme. When the total energy and the residuals satisfy the convergence criterion, we return to the force calculation step.

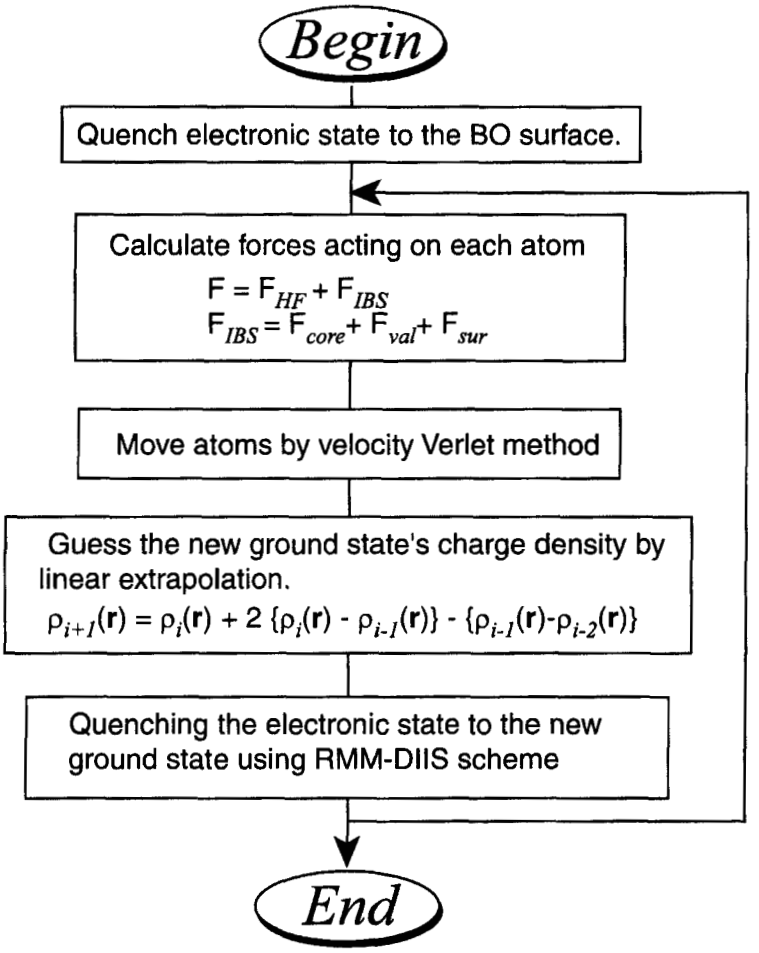

FIGURE 4 Flowchart of the LAPW-MD calculation.

6. NUMERICAL EXAMPLES

6.1. H_2

We choose the H_2 molecule as a first test case of the new LAPW-MD method. A simple cubic (SC) supercell of volume 1000 a.u.^{3} is used and two hydrogen atoms are initially placed along the z-axis with 1.4 a.u. interatomic distance. The MT radius R_{MT} for H atom is chosen as 0.65 a.u.. Only the Γ-point is included in the k-point sampling. The cut-off energies for the wave function and the potential energy are taken to be 40 Ry. and 160 Ry. respectively. This choice of the cut-off energy for the wave

functions yields 4337 LAPW's and corresponds to $R_{MT}K_{max} = 4.1$. Inside the MT sphere, the angular momentum expansion for the wave function, charge density and potentials are truncated at $l_{max} = 6$. It is a reasonable choice, because higher angular momentum components of the charge density and potentials of such a small MT radius is very small. The Vosko–Wilk–Nusair's [25] parameterized exchange-correlation functional is used. Before starting the wave function optimization using RMM-DIIS method, we carried out a single iteration of the block Davidson method in order to provide a better initial wave functions.

Next, we studied the motion of hydrogen atoms using molecular dynamics method. The time step is 20 a.u. and no temperature control method is employed (*i.e.*, microcanonical ensemble). From the observation of the atomic motions, the vibrational frequency and equilibrium distance are determined as 1.45 a.u. and 4306 cm^{-1} respectively. These values are reasonably close to the experimental values of 1.40 a.u. and 4403 cm^{-1}.

6.2. O_2

As a test for the open shell system, the triplet ground state of a molecular oxygen is studied. Initially, two oxygen atoms are aligned on one of a vertices of the 1000 a.u.^{3} SC supercell at 2.30 a.u. interatomic distance. The MT radius is chosen as 1.1 a.u. and the number of radial mesh points (logarithmic mesh) is set to 351. The energy cut-off of 30 Ry. is applied for wave functions, corresponding to 2777 LAPW's and $R_{MT}K_{max} = 6.0$. We first obtained the triplet electronic ground state for the initial configuration. Then we performed a MD simulation with $\Delta t = 100$ a.u. and obtained the vibrational frequency and equilibrium distance to be 1531 cm^{-1} and 2.31 a.u. respectively. The vibrational frequency was determined from the oscillation curve of the total force depicted in Figure 5. In Table I, we summarize the present result and compared to experimental value and other calculations. The deviation from the experiment is less than 2% in the equilibrium distance and 4% in the vibrational frequency.

6.3. Mo_2

As an example of the LAPW-MD calculation on transition metal elements, we investigated the structure and dynamics of Mo_2 diatomic molecule. A symmetry-broken ground state electronic structure is one of an attractive feature of Mo_2 diatomic molecule. The spatial spin density distribution of

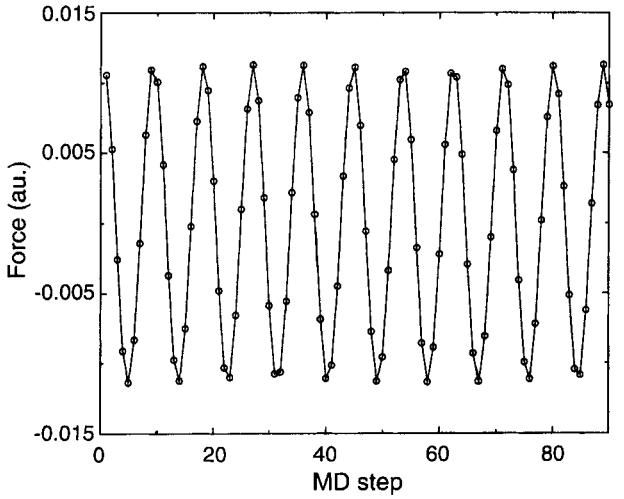

FIGURE 5 The time evolution of total force for O_2 molecule obtained from LAPW-MD calculation.

TABLE I Comparisons of the equilibrium distance and vibrational frequency of O_2

	LCAO[a]	*LMTO*[b]	*Present work*	*Experiment*[c]
R_e(a.u.)	2.34	2.47	2.31	2.28
ω_e(cm^{-1})	1590	1467	1531	1580

[a] Ref. [27].
[b] Ref. [28].
[c] Ref. [29].

the Mo_2 exhibits broken-symmetry ($C_{\infty v}$) at the interatomic distance larger than the equilibrium distance [26]. The antiferromagnetic pattern of the spin density is a consequence of strong correlation interaction between the electrons of each Mo site.

At first, Mo atoms are placed along a vertex of a 5832 a.u.^{3} SC supercell at a 3.7 a.u. interatomic distance. The MT radius and radial mesh point is chosen as 1.8 a.u. and 451 respectively. Due to the small MT radius, 4*p* core orbitals are treated as semi-core states. A relativistic calculation is employed inside the MT spheres, because the relativistic effect becomes important in the case of heavy elements. Wave function expansion is truncated at 8 Ry. cut-off energy ($R_{MT}K_{max} = 7.2$). The initial broken symmetry wavefunctions for α and β-spin are constructed by a random number generator. The calculated equilibrium distance and vibrational frequency are 3.86 a.u. and 424 cm^{-1}, respectively. We compare the LAPW-MD result with experiment and other calculation in Table II. The equilibrium distance in

TABLE II Comparisons of the equilibrium distance and vibrational frequency of Mo_2

	LCAO[a]	*Present work*	*Experiment*[b]
R_e(a.u.)	1.97	2.04	1.938
ω_e(cm^{-1})	423	424	477.1

[a] Ref. [26].
[b] Ref. [30].

the present calculation is about 5% larger than the experiment, whereas vibrational frequency is very close to the LCAO result and both results underestimate the vibrational frequency by 11%.

7. PARALLEL EFFICIENCY

We have investigated parallel efficiency of our LAPW-MD program code. Parallelization of the code is achieved in two ways. The first method uses SGI Fortran77 compiler's automatic parallelization function, and the other employs the Message Passing Interface (MPI) protocol. In these calculations, we have used the SGI Origin2000 32 processor shared memory computer.

No difficulty was encountered in the automatic parallelization, we need only to insert some compiler options in the code. The SGI Fortran77 compiler divides "DO loops" into blocks and allocates one of these to separate processor. The MPI parallelization requires some efforts to implement, because it is essential to know which part of the code can be parallelized efficiently or not. The most time consuming part of the program is the quenching process of the wave functions. In most solid state band structure calculations, efficient parallelization can be achieved by dividing the loop over k-points. However, when a calculation involves small k-point set (*e.g.*, cluster, large supercell box *etc.*), the k-point division strategy is not too efficient.

Our implementation of the MPI parallelization was accomplished by dividing the band loops. At the DO loop statement for bands, the loop counter increment is set to be the number of processors and a number of bands are assigned to each processor. Before entering into the band loop, each processor has the same data (*e.g.*, wave function, charge density *etc.*). Inside the band loop, each processor has different data, because the bands assigned to different processor are separately quenched and updated. After quenching a band, each processor broadcasts the wavefunction to the other processor, and finally, all of the processors share same memory image. This procedure makes program coding very simple, but the memory

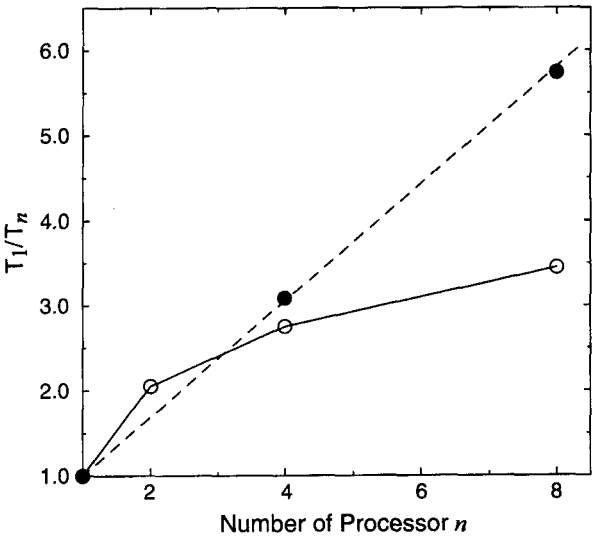

FIGURE 6 The time ratio of single CPU run and parallel run for MPI implementation (filled circle) and SGI's pfa automatic parallelization (open circle).

requirement increases linearly with respect to the number of processors. In the RMM-DIIS and Davidson iterative diagonalization scheme, each band is quenched independently and no explicit orthonormalization process is required during the band loop, so the data transfer between processors is kept small. Therefore, it is expected that good performance and scalability with respect to the number of processors will be achieved.

Figure 6 shows the speedup of the parallel calculation on a 8 atom supercell calculation of diamond Si. Here the speedup is defined by the time ratio between n-processors and a single processor calculation. The curve for the automatic parallelization is almost saturated at 8-processors and no gain is expected for more than 8-processors. On the other hand, the MPI parallelization results show an almost linear trend with respect to the number of processors. At 8-processor the performance gain by the MPI parallelization is 1.66 times larger than that of the automatic parallelization.

8. CONCLUSION

We have implemented the iterative diagonalization scheme for LAPW electronic structure calculation and extended the method to AIMD calculations. It was pointed out that the RMM-DIIS scheme has several

advantages over the conventional Car-Parrinello type iterative diagonalization scheme in the case of LAPW basis set. We have shown that the AIMD calculations using the LAPW basis set applied to some diatomic molecule yield good results for the equilibrium distances and vibrational frequencies. The parallelization of the program code based on the band parallel strategy using MPI exhibited excellent scalability with respect to the number of processors. It is expected that more large scale LAPW-MD calculations will be realized using the iterative diagonalization scheme and more powerful parallel computers in near future.

Acknowledgements

The authors wish to thank Prof. Y. Hiwatari at Kanazawa Univ. for continuous help and useful discussion. One of the author, K. U., gratefully appreciate NSERC financial support during his postdoctoral fellowships period.

References

[1] Andersen, O. K. (1975). "Linear methods in band theory", *Phys. Rev. B*, **12**, 3060.
[2] Singh, D. J., "*Planewaves, Pseudopotentials and the LAPW method*", Kluwer Academic Publishers, Boston, Dordrecht, London, 1994.
[3] Hohenberg, P. and Kohn, W. (1964). "Inhomogeneous electron gas", *Phys. Rev.*, **136**, 864.
[4] Kohn, W. and Sham, L. J. (1965). "Self-consistent equations including exchange and correlation effects", *Phys. Rev.*, **140**, 1133.
[5] Lundqvist, S. and March, N. H., "*Theory of the inhomogeneous electron Gas*", Plenum, New York, 1983.
[6] Jones, R. O. and Gunnarsson, O. (1989). "The density functional formalism, its applications and prospects", *Rev. Mod. Phys.*, **61**, 689.
[7] Jansen, H. J. F. and Freeman, A. J. (1984). "Total-energy full-potential linearized augmented-plane-wave method for bulk solids: Electronic and structural properties of tungsten", *Phys. Rev. B*, **30**, 561.
[8] Mattheiss, L. F. and Hamman, D. R. (1986). "Linear augmented-plane-wave calculation of the structural properties of bulk Cr, Mo and W", *Phys. Rev. B*, **33**, 823.
[9] Jepsen, O., Andersen, O. K. and Mackintosh, A. R. (1975). "Electronic structure of hcp transition metals", *Phys. Rev. B*, **12**, 3084.
[10] Weinert, M., Wimmer, E. and Freeman, A. J. (1982). "Total-energy all-electron density functional method for bulk solids and surfaces", *Phys. Rev. B*, **26**, 4571.
[11] Singh, D., Yu, R. and Krakauer, H. (1990). "All-electron and pseudopotential force calculations using the linearized-augmented-plane-wave method", *Phys. Rev. B*, **43**, 6411.
[12] Car, R. and Parrinello, M. (1985). "Unified approach for molecular dynamics and density-functional theory", *Phys. Rev. Lett.*, **55**, 2471.
[13] Payne, M. C., Teter, M. P., Allan, D. C., Arias, T. A. and Joannopoulos, J. D. (1992). "Iterative minimization techniques for *ab initio* total-energy calculations: molecular dynamics and conjugate gradients", *Rev. Mod. Phys.*, **64**, 1045.
[14] Bylander, D. M. (1990). Leonard Kleinmann and Seongbok Lee, "Self-consistent calculations of the energy bands and bonding properties of $B_{12}C_3$", *Phys. Rev. B*, **42**, 1394.
[15] Wood, D. M. and Alex Zunger (1985). "A new method for diagonalising large matrices", *J. Phys. A*, **18**, 1343.

[16] Pulay, P. (1980). "Convergence acceleration of iterative sequences. The case of SCF iteration", *Chem. Phys. Lett.*, **73**, 393.
[17] Pulay, P. (1982). "Improved SCF convergence acceleration", *J. Comp. Chem.*, **3**, 556.
[18] José Luís, Martins and Marvin L., Cohen (1987). "Diagonalization of large matrices in pseudopotential band-structure calculations: Dual-space formalism", *Phys. Rev. B*, **37**, 6134.
[19] Goedecker, S. and Maschke, K. (1990). "Alternative approach to separable first-principles pseudopotentials", *Phys. Rev. B*, **42**, 8858.
[20] Goedecker, S. and Maschke, K. (1991). "Operator approach in the linearized augmented-plane-wave method: Efficient electronic-structure calculations including forces", *Phys. Rev. B*, **45**, 1597.
[21] MacDonald, A. H., Pickett, W. E. and Koelling, D. D. (1980). "A linearized relativistic augmented-plane-wave method utilizing approximate pure spin basis functions", *J. Phys. C*, **13**, 2675.
[22] Press, W. H., Teukolsky, S. A., Vetterling, W. T. and Flannery, B. P., "*Numerical recipes in FORTRAN: the art of scientific computing*", Cambridge University press, New York, 1992.
[23] Tassone, F., Mauri, F. and Car, R. (1994). "Acceleration scheme for *ab initio* molecular-dynamics simulations and electronic-structure calculations", *Phys. Rev. B*, **50**, 10 561.
[24] Singh, D., Henry Krakauer and Wang, C. S. (1986). "Accelerating the convergence of self-consistent linearized augmented-plane-wave calculations", *Phys. Rev. B*, **34**, 8391.
[25] Vosko, S. H., Wilk, L. and Nusair, M. (1980). "Accurate spin-dependent electron liquid correlation energies for local spin density calculations: a critical analysis", *Can. J. Phys.*, **58**, 1200.
[26] Baykara, N. A., McMaster, B. N. and Salahub, D. R. (1984). "LCAO local-spin-density and Xα calculations for Cr_2 and Mo_2", *Mol. Phys.*, **52**, 891.
[27] Kitaura, K., Satoko, C. and Morokuma, K. (1979). "Total energies of molecules with the local density functional approximation and Gaussian basis sets", *Chem. Phys. Lett.*, **65**, 206.
[28] Gunnarsson, O., Harris, J. and Jones, R. O. (1977). "Density functional theory and molecular bonding I. First-row diatomic molecules", *J. Chem. Phys.*, **67**, 3970.
[29] Herzberg, G., "*Electronic spectra of polyatomic molecules*", Van Nostrand, Princeton, 1950.
[30] Morse, M. D. (1986). "Clusters of transition-metal atoms", *Chem. Rev.*, **86**, 1049.